Solid Earth Discuss., 5, 2345–2388, 2013
www.solid-earth-discuss.net/5/2345/2013/
doi:10.5194/sed-5-2345-2013

Solid Earth
Discussions
Open Access

Comparing a thermo-mechanical Weichselian ice sheet reconstruction to GIA driven reconstructions: aspects of earth response and ice configuration

P. Schmidt[1], B. Lund[1], and J-O. Näslund[2]

[1]Department of Earth Sciences, Uppsala University, Villavägen 16, 752 36 Uppsala, Sweden
[2]Swedish Nuclear Fuel and Waste Management Company (SKB), P.O. Box 250, 101 24 Stockholm, Sweden

Received: 27 November 2013 – Accepted: 29 November 2013 – Published: 17 December 2013

Correspondence to: P. Schmidt (peter.schmidt@geo.uu.se)

Published by Copernicus Publications on behalf of the European Geosciences Union.

Abstract

In this study we compare a recent reconstruction of the Weichselian ice-sheet as simulated by the University of Main ice-sheet model (UMISM) to two reconstructions commonly used in glacial isostatic adjustment (GIA) modeling: ICE-5G and ANU (also known as RSES). The UMISM reconstruction is carried out on a regional scale based on thermo-mechanical modelling whereas ANU and ICE-5G are global models based on the sea-level equation. The Weichselian ice-sheet in the three models are compared directly in terms of ice volume, extent and thickness, as well as in terms of predicted glacial isostatic adjustment in Fennoscandia.

The three reconstructions display significant differences. UMISM and ANU includes phases of pronounced advance and retreat prior to the last glacial maximum (LGM), whereas the thickness and areal extent of the ICE-5G ice-sheet is more or less constant up until LGM. The final retreat of the ice-sheet initiates at earliest time in ICE-5G and latest in UMISM, while ice free conditions are reached earliest in UMISM and latest in ICE-5G. The post-LGM deglaciation style also differs notably between the ice models. While the UMISM simulation includes two temporary halts in the deglaciation, the later during the Younger Dryas, ANU only includes a decreased deglaciation rate during Younger Dryas and ICE-5G retreats at a relatively constant pace after an initial slow phase. Moreover, ANU and ICE-5G melt relatively uniformly over the entire ice-sheet in contrast to UMISM which melts preferentially from the edges.

We find that all three reconstructions fit the present day uplift rates over Fennoscandia and the observed relative sea-level curve along the Ångerman river equally well, albeit with different optimal earth model parameters. Given identical earth models, ICE-5G predicts the fastest present day uplift rates and ANU the slowest, ANU also prefers the thinnest lithosphere. Moreover, only for ANU can a unique best fit model be determined. For UMISM and ICE-5G there is a range of earth models that can reproduce the present day uplift rates equally well. This is understood from the higher present day uplift rates predicted by ICE-5G and UMISM, which results in a bifurcation in the

best fit mantle viscosity. Comparison of the uplift histories predicted by the ice-sheets indicate that inclusion of relative sea-level data in the data fit can reduce the observed ambiguity.

We study the areal distributions of present day residual surface velocities in Fennoscandia and show that all three reconstructions generally over-predict velocities in southwestern Fennoscandia and that there are large differences in the fit to the observational data in Finland and northernmost Sweden and Norway. These difference may provide input to further enhancements of the ice-sheet reconstructions.

1 Introduction

Fennoscandia has been a key area in the development of theories and models of glacial isostatic adjustment (GIA) due to the unique temporal and spatial coverage of observational data (e.g. Ekman, 1991) and the region remains an important study area, see summaries of recent work in e.g. Plag et al. (1998), Whitehouse (2009) and Steffen and Wu (2011). Much GIA work has aimed at determining a model of the Weichselian ice-sheet, which covered Fennoscandia during the last glacial period, and better knowledge of the rheological properties of the Earth beneath Fennoscandia. Today several reconstructions of the Weichselian ice-sheet are available, both regional models and as part of global models. The two main geometrical properties of an ice-sheet, the areal extent and the distribution of ice thickness, are very different in terms of how difficult they are to constrain. The areal extent can usually be reasonably well determined from geological markers such as moraines. For the ice thickness no such data is available and it therefore has to be determined by indirect methods.

Ice-sheet reconstructions can broadly be categorized into two groups. The first, classical approach base the reconstruction primarily on geological markers of the extent of the ice-sheet at different times. The ice thickness is then adjusted such that the solution to the sea level equation fits available GIA data (mainly relative sea-level (r.s.l.) and tide-gauge data, but more recently also GPS data). For global models, estimates of the eustatic sea level are used to constrain the total volume of ice at different times. Early models of this type did not extend further back in time than to the last maximum extent of the ice-sheet, due to sparsity of older r.s.l. data and geological markers. Of the reconstructions used in this study, ICE-5G (Peltier, 2004) and ANU (Lambeck et al., 2010) both belong to the first group.

The second group reconstruct ice-sheets from physical (thermodynamical) principles, often using palaeo climate data to govern the evolution of the ice-sheet. This provides an ice-sheet which behaves as a real ice-sheet in terms of basal sliding, ice streams, ice thickness distribution and growth and decay properties. Geological markers and r.s.l. data may be used to constrain the reconstruction. UMISM (Näslund, 2010) is an example of this type of model. As the interdependence between ice model and earth model varies in the two types of reconstructions, they may provide complementing information on the properties of the Earth.

In this study we compare a recent thermo-mechanical reconstruction of the Weichselian ice-sheet, UMISM (Näslund, 2010), with two models constrained by geological markers and relative sea level (r.s.l.) observations: ANU (Lambeck et al., 2010, also known as RSES) and ICE-5G (Peltier, 2004). An earlier version of ANU (Lambeck et al., 1998) has previously been compared to ICE-5G by Steffen et al. (2010) using satellite based gravity data (GRACE). That study focused on the use of GRACE data in GIA modelling and concluded that both models are adequate for studying the GIA process in Fennoscandia. Here we add a third ice-sheet reconstruction to the comparison as well as an updated version of ANU. We compare the three ice models both directly in terms of the ice-sheet history as well as in terms of post-glacial uplift and present day uplift rates predicted by GIA modeling. For an assessment of optimal earth model parameters for the three reconstructions we compute the misfit to present day uplift rates measured by GPS (Lidberg et al., 2007) and compare the predicted postglacial uplift to r.s.l. observations along the Ångerman river, Sweden (Lidén, 1938; Cato, 1992).

2 Ice sheet reconstructions

Observations of the post-glacial GIA process as well as geological markers are usually dated using the C-14 method. Most of the early reconstructions are therefore given in C-14 years rather than calender years. As these two timescales differ by up to 3.5 kyr around the time of the last glacial maximum (Bard et al., 1990) it is important to note that all three reconstructions considered here, as well as all observational data used herein is dated in calender years.

2.1 Last Glacial Maximum

An event commonly referred to when discussing ice-sheet reconstructions is the last glacial maximum, LGM. This often refers to the last maximum advance of the ice-sheet. However, the conditions governing the advance and retreat of an ice-sheets will vary from place to place. Therefore the maximum advance will not be a synchronous event in all parts of a large ice-sheet. In the case of the Weichselian ice-sheet the time span enclosing the last maximum advance may be as long as 10 kyr years (e.g. Boulton et al., 2001).

In this study we have chosen to define LGM as the point in time of the last occurrence of the maximum volume of the ice-sheet, remembering that this may not coincide with the maximum areal extent, thickness or advance of the ice front.

2.2 UMISM

The UMISM ice-sheet reconstruction (Näslund, 2010) uses the October 2004 version of the thermo-mechanical University of Maine ice-sheet model (Fastook and Chapman, 1989; Fastook, 1994; Fastook and Prentice, 1994). UMISM was part of the “European ice-sheet modeling initiative model inter-comparison experiment” and yielded output in agreement with other thermodynamic ice-sheet models (Huybrechts et al., 1996; Payne et al., 2000). The reconstruction has previously been used in GIA modeling for assessment of shoreline migration (Whitehouse, 2006) as well as fault stability (Lund et al., 2009).

In the present simulation UMISM was used for a relatively high resolution, regional scale, reconstruction of the Weichselian ice-sheet on an equidistant (50 km × 50 km) grid every 100 yr since 120 kyr before present (BP). The ice-sheet constitutes three main sub-systems: mass-balance, ice movement, and ice temperature for which the model solves the conservation of mass, momentum, and energy equation, respectively. The UMISM model used for the present reconstruction uses the shallow-ice approximation for solving stresses and ice velocities. The model includes a sub-glacial hydrology model (Johnson, 1994) that transports melt water under the ice-sheet according to prevailing pressure potentials, governed by ice-sheet thickness and basal topography. The response of the solid Earth is modeled in a simplified way using a hydrostatically supported elastic plate model, adequate for the purpose of placing the ice-sheet surface at an appropriate altitude, and hence obtaining an appropriate air temperature for the ice surface mass balance calculation.

The simulation is run using a palaeo-temperature record, from which the spatial pattern of air temperature is obtained and precipitation is calculated through a mass balance relationship, developed from the Antarctic ice-sheet (Fastook and Prentice, 1994). This precipitation is further dependent on distance from the pole, saturation vapor pressure (function of altitude and lapse-rate), and surface slope. As a proxy for the air temperature record, data for the last 120 kyr from the Greenland ice core project (Dansgaard et al., 1993) has been used. The ice-sheet reconstruction was calibrated against dated ice-marginal positions for Weichselian stadials (e.g. Lokrantz and Sohlenius, 2006) by making slight systematic adjustments to the temperature curve (Näslund, 2010). This ice-sheet calibration process did not focus on the northern ice-sheet margins, resulting in a major uncertainty in ice margin position around e.g. the Barents Sea. For the basal boundary conditions the ETOPO2 digital elevation model was used as well as the geothermal heat flux model by Näslund et al. (2005). An estimated eustatic sea-level curve from a previous UMISM reconstruction of all Northern Hemisphere ice-sheets was used for determining the changes in position of the ice-sheet grounding-line (constraining terrestrial parts of the ice-sheet).

2.3 ICE-5G (VM2)

The global ICE-5G model (Peltier, 2004) is built upon successive refinements of models of the last Pleistocene deglaciation. The initial model in the suite, ICE-1 (Peltier and Andrews, 1976), tabulated ice thicknesses of the Laurentide, Greenland and Fennoscandian ice-sheets from 18 kyr BP and onward. Updates include the widely used ICE-3G (Tushingham and Peltier, 1991) and ICE-4G (Peltier, 1994) models. A new model (ICE-6G) is under development (Toscano et al., 2011) but has so far not been made publically available.

The ICE-n suite are global models based on dated observations of ice-sheet margins, r.s.l. curves and the eustatic sea level curve. As such, the ICE-n models critically depend on the use of the sea level equation to compute r.s.l. estimates. ICE-1 was based on analytical relations between the distance from the ice margin and the ice thickness, assuming dynamical equilibrium of the ice-sheet, as well as estimates of the ice history in some central areas considered critical. In later versions the ice thicknesses have been manually adjusted to optimize the fit to the growing body of observational constraints. Of the individual ice-sheets, Antarctica is the least well constrained in that no or very little adequate data are available from this continent (Peltier, 1998). Therefore, Antarctica has mainly been used as a buffer to ensure that the fit to the observed eustatic sea level is maintained, as well as the fit to the sparse sample of r.s.l. records from the southern ocean.

Parallel to the ICE-n development, the VMn mantle viscosity models have been developed using GIA modeling constrained by r.s.l. data, rebound relaxation spectra, Earth rotation anomalies and polar wander (Peltier, 1996, 1998). In the inversion for the VMn models, the ICE-n models have been used as predefined loading. The derived viscosity models have then been used in constructing the next generation ICE-n models.

SED
5, 2345–2388, 2013

The latest published version of the ICE-n suite is the ICE-5G (VM2) model (Peltier, 2004). The theoretical framework and methodology of ICE-5G is the same as that employed for its closest predecessors, but the viscosity structure of the earth model has been updated to the more advanced VM2 model (Fig. 1), which was constructed based on the ICE-4G model (Peltier, 1996). In the original VM2 model the elastic thickness of the lithosphere was prescribed to 120.6 km, this was however reduced to 90 km in the ICE-5G reconstruction to better fit GIA data from the British Isles. We note that VM2 has a mean viscosity of about 5×10^{20} Pa s in the upper mantle and about 1.6×10^{21} Pa s in the uppermost part of the lower mantle.

Peltier and Fairbanks (2006) presented an extension of ICE-5G to 120 kyr (BP), based on the SPECMAP δ^{18}O record by Martinson et al. (1987). In this study we use the extended version of ICE-5G (VM2) which is sampled on an approximately $0.7^{\circ} \times 0.7^{\circ}$ grid with a temporal resolution of 500 yr from 17 kyr BP to present, 1 kyr between 32–17 kyr BP and 2 kyr at earlier times. For simplicity we will in what follows refer to this model as ICE-5G rather than ICE-5G (VM2).

2.4 ANU

The ANU model, also known as RSES, is best considered a collection of models of individual ice-sheets, together comprising a global model. As in the case of the ICE-n suite, the ANU model has been developed in a series of papers, starting with Nakada and Lambeck (1987, 1988, 1989). However, in contrast to the ICE-n models, where the entire global model is updated, ANU has evolved from successive reconstructions of individual ice-sheets.

The first version used ICE-1 and ICE-2 for the Laurentide and Fennoscandian ice-sheets, constrained in the Barents and Kara sea by the model by Hughes et al. (1981), while models of the deglaciation of Antarctica were constructed based on the work by Hughes et al. (1981), Drewry (1982) and Wu and Peltier (1983). A regional model of the British ice-sheet was added by Lambeck (1993, 1995) and the Fennoscandian ice-sheet was modified in Lambeck et al. (1998).

SED
5, 2345–2388, 2013

The latest ANU model was presented in Lambeck et al. (2010). This revision present a new reconstruction of the Fennoscandian ice-sheet with exception for the Barents and Kara sea region, where the solution from Lambeck (1996) is used. An new reconstruction of the Laurentide ice-sheet has also been generated (Lambeck et al., 2010) although not yet published. For the period preceding LGM the reconstruction is mainly controlled by available data on ice-sheet margins and an assumption of ice-sheet basal conditions equal to those at LGM. At times prior to 64 kyr BP the reconstruction by Lambeck et al. (2006) is used. Loading of ice-lakes and marine limit data have been added to the computation and the density structure and elastic parameters of the Earth are adopted from PREM (Dziewonski and Anderson, 1981).

In the reconstruction the sea level equation is solved, constrained by geological markers of ice-sheet extent and r.s.l. data. As a starting model, ice thicknesses are computed from simple glaciological assumptions leading to analytical expressions for the relation between the thickness, distance from the margin and basal shear stress (Paterson, 1994), with basal stress determined from the reconstruction between 23–21 kyr BP in Lambeck et al. (2006). The final solution is obtained through a series of iterations involving fit to different parts of the constraining data set or introduction of new data while optimizing either via a spatially and temporally varying scale factor or via the earth model parameters. Therefore, in addition to the Weichselian ice-sheet reconstruction, this scheme also produces an estimate of the elastic thickness of the lithosphere (65–100 km) and the viscosity of the upper and lower mantle beneath Fennoscandia ($3–4 \times 10^{20}$ and $5–20 \times 10^{21}$ Pa s, respectively, Fig. 1). This can be compared to the ICE-5G reconstruction where the Earth structure is assumed known prior to the reconstruction. The spatial resolution of the model is 0.5° in longitude and 0.25° in latitude. In time the model is sampled on varying length intervals (450–5000 yr), capturing the timing of important changes in the evolution of the ice-sheet.

3 Comparison of the ice-sheet reconstructions

In this section we compare the three ice-sheet reconstructions directly, first in terms of integrated quantities such as of volume, area and mean thickness, after which we look more closely at the details of the reconstructions at LGM and a few selected post-LGM snapshots. We will compare the ice-sheet reconstructions from 69 kyr BP onward since the UMISM model is less well constrained at prior times.

3.1 Ice volumes, areal extent and thickness

A comparison of ice volume, areal extent, mean and maximum thickness of the three ice-sheet reconstructions is shown in Fig. 2. In terms of volume and areal extent we see that both ANU and UMISM display a period of small ice-cover preceding LGM by some 13–16 kyr, while ICE-5G only displays minor fluctuations in volume and nearly constant areal extent pre-LGM. LGM in ICE-5G occurs at 26 kyr BP although the decline in volume up until 21 kyr BP is only about 7 % while the areal extent over the same period is more or less constant. In ANU and UMISM LGM occurs at 21 and 18.2 kyr BP respectively, but we note that the maximum areal extent occurs slightly earlier (21 533 and 18 400 yr BP respectively). In general, UMISM has the smallest areal extent and ICE-5G the largest. During its two periods of extensive ice-sheets, UMISM displays the greatest mean thickness of the three ice models, indicating that the style of accumulation and ablation in this reconstruction is significantly different from ANU and ICE-5G. Specifically, the initially increasing mean thickness during periods of deglaciation indicate that the ice-sheet melts preferentially from the edges and inwards in UMISM, whereas the correlation between mean thickness, ice volume and extent in ANU and ICE-5G indicates that the ice melts more or less uniformly over the ice-sheet in these reconstructions. Interestingly, the greatest thickness in UMISM occurs some 3.9 kyr after LGM.

A notable difference between the reconstructions during deglaciation is a 2 kyr long hiatus in UMISM some 1.5 kyr after LGM. This is followed by very rapid deglaciation

SED
5, 2345–2388, 2013

until Younger Dryas, at about 13 kyr BP, when the ice-sheet increases slightly both in volume and extent (Fig. 2). Neither ICE-5G nor ANU displays the hiatus or the growth seen in UMISM, although the deglaciation rate is notably impeded in ANU from about 2 kyr years prior to Younger Dryas. In ANU the deglaciation rate increases again after Younger Dryas while in ICE-5G the deglaciation continues at approximately unchanged rate until the end of glaciation.

3.2 Ice sheets at LGM

Snapshots of the Weichselian ice-sheet reconstructions at LGM can be seen in Fig. 3. We see that the maximum thickness in UMISM is centered over the Gulf of Bothnia, whereas the maximum thickness in ANU and ICE-5G, at their respective LGM, is located slightly further south. Both ANU and ICE-5G display double ice domes over Fennoscandia with one of the domes approximately co-located with the present day center of uplift. In ICE-5G the second dome is located over the northern part of the Gulf of Bothnia while in ANU it is located just north-west of lake Vänern, close to the border between Norway and Sweden. To the north, ANU and ICE-5G show extensive ice-sheets over the Barents and Kara seas, whereas UMISM mainly shows ice coverage in an area east of Svalbard.

From Norway toward the British Isles, both ICE-5G and UMISM have a connecting ice-bridge, albeit thinner and wider in the case of ICE-5G. In ANU no such feature is seen in Fig. 3, although a continuous ice-sheet from Norway to the British isles exists in ANU between 29.5 and 27 kyr BP. A notable thinning of ice in ICE-5G is seen across a NE–SW divide running parallel to the southern shoreline of Finland down through south-central Sweden. Such a feature is absent in ANU and UMISM. Southeast of the divide, ICE-5G is significantly thinner than ANU and UMISM. At LGM the ice edge is located slightly further inland over the Baltic countries in ANU and ICE-5G than in UMISM, and offshore Norway, ICE-5G extends further out with greater thicknesses than ANU and UMISM.

3.3 Post-LGM ice-sheets

The post-LGM ice-sheets in the three reconstructions can be seen at three selected times in Fig. 4. Over Fennoscandia the areal extents of the ice-sheets agree well, although differences in the timing of the end of glaciation differs slightly with ice free conditions at 10 100 BP in UMISM, 9650 BP in ANU and 8 kyr BP in ICE-5G. The non-zero thickness until present day in ICE-5G seen in Fig. 2 is associated with a non-vanishing small ice-cover in the northernmost part of Novaya Zemlya, Russia. Similar to the ice-sheets at or just prior to LGM, we see that ICE-5G and UMISM have the greatest thickness over the Gulf of Bothnia, whereas ANU displays two local maxima further south. We also note that in the last stages of ice retreat, the ice has migrated into the mountains in UMISM while in ICE-5G it is centered on the Bay of Bothnia and in ANU over inland northern Sweden.

4 Glacial Isostatic Adjustment modeling

To model the GIA process we need two components: an ice model and an earth model. Collectively we refer to these as a GIA model. Combined with observational data, GIA modelling makes it possible to infer rheological properties of the Earth, such as the elastic thickness of the lithosphere and the viscosity structure of the mantle. However, since many ice models require an earth model for the reconstruction of ice thickness, the two are often not independent.

4.1 Earth model implementation

Our GIA model is implemented in the commercially available finite element (FE) code Abaqus, following the recipe of Wu (2004). We use the incompressible flat-earth approximation and neglect self-gravitation. This scheme was benchmarked by Schotman et al. (2008). They found that the predicted vertical displacements rates agree well with those of an incompressible self-gravitating spectral model while the horizontal dis-

SED
5, 2345–2388, 2013

Title Page
Abstract Introduction
Conclusions References
Tables Figures
◀◀ ▶▶
◀ ▶
Back Close
Full Screen / Esc
Printer-friendly Version
Interactive Discussion

placement rates were generally larger unless material compressibility was included in the finite element model. We therefore include material compressibility in our model but choose not to put too much emphasis on the predicted horizontal velocities in our analysis. An early version of our model was benchmarked in Spada et al. (2011), confirming the conclusions in Schotman et al. (2008). The model has since then been updated following Schmidt et al. (2012).

The central part of our FE model covers the formerly glaciated Fennoscandian and Barents Sea regions, with a resolution of 50 × 50 km horizontally, identical to that of UMISM. Further out we expand the model to a half-sphere of radius about 10 times the central region using a coarser mesh. Material boundaries in terms of density and elastic parameters are included at 15 km and 50 km depth, at the base of the elastic lithosphere and at 410 km and 670 km, using PREM (Dziewonski and Anderson, 1981) volume averages as summarized in Table 1. In what follows we will vary the thickness of the elastic lithosphere and the viscosity of the mantle.

4.2 Ice sheet implementation

The ice-sheet over Fennoscandia, the British Isles and the Barents and Kara seas is implemented as a pressure source in the GIA models. We transfer the spatial sampling of ICE-5G and ANU to that of the earth model by bilinear interpolation. Thus the earth models loaded by different ice models will use the same mesh, and differences in predicted displacements will only depend on differences in the load history, for earth models with identical layering and material parameters.

As the ice models are sampled at different time intervals we use the closest available snapshot in time after 69 kyr BP to initialize the ice load (Fig. 2). During the simulations we assume linear growth and decay of ice thicknesses between adjacent times, while the areal extent is assumed constant at the value of the closest preceding snapshot. The latter assumption is motivated from the fact that the ice-thickness either grows from zero thickness or decays to zero thickness in the cells differing between two frames. Hence the assumption leads to a smooth evolution of the ice-sheet.

SED
5, 2345–2388, 2013

To test whether or not excluding the ice history prior to 69 kyr BP affects the post glacial uplift we have constructed a hybrid ice model using the ICE-5G ice-sheet at times earlier than 36 kyr BP and the ANU reconstruction from there on to present day. The present day uplift rates predicted by this hybrid ice-sheet differ by less than 0.1 mm yr^{-1} from those predicted by the original ANU model. Given the large difference between ICE-5G and ANU prior to 36 kyr BP (Fig. 2) this indicates that the ice-history before 69 kyr BP has a negligible influence on the present day uplift rates.

4.3 Observational data

We compare the predicted displacement rates from our GIA models to present day GPS data, collected and analyzed in the BIFROST project (Lidberg et al., 2007), see Fig. 5. The formal uncertainties in this data set are in the range 0.15–1.13 mm yr^{-1} (mean 0.29 mm yr^{-1}) for the vertical velocities and 0.04–0.26 (mean 0.09 mm yr^{-1}) for the horizontal velocities. In this study we focus on the vertical component, but we also present predicted horizontal displacement rates in the residual velocity plots (adjusted by a rigid rotation, see Lidberg et al., 2007, for a discussion).

A more recent processing of the BIFROST project GPS data, which includes more stations and longer time series, is also available (Lidberg et al., 2010). We note that the displacement rates differ between the two realizations by up to approximately 1 mm yr^{-1}, with generally greater velocities in both the vertical and horizontal components of the more recent processing. As the major difference between the two solutions is the choice of reference frame (ITRF2000 vs. ITRF2005), this indicates that the uncertainties in reality are of the order of 1 mm yr^{-1} due to the reference frame realization (Lidberg et al., 2010). As the objective of this study is not focused on finding the optional earth model parameters but rather study the difference between the three ice-reconstructions the choice of which processing to use is not of major importance. Here we will use the 2007 realization as the primary observational data and only briefly comment on the fit of the model predictions to the 2010 realization.

SED
5, 2345–2388, 2013

The fit of the model predictions to the GPS data is computed using the normalized chi-squared value

$$\chi_\nu^2 = \frac{1}{N-M}\sum_{i=0}^{N}\left(\frac{v_i^{\mathrm{mod}} - v_i^{\mathrm{obs}}}{\sigma_i}\right)^2 \tag{1}$$

where v_i^{mod} and v_i^{obs} are the vertical velocities predicted by the model and observed by GPS respectively, σ_i are the uncertainties of the observed velocities, N is the number of data points and M the number of free parameters in the GIA model (in this study the lithospheric thickness and the mantle viscosity).

In addition to GPS data, we compare the predicted post glacial uplift to the classic relative sea level data collected along the Ångerman river at the northeastern coast of Sweden (Lidén, 1938; Cato, 1992) and close to the former center of the ice-sheet. However, as we do not solve the sea level equation, nor compute geoid heights in our model, a comparison between our model data and r.s.l. data must be made with caution. We will therefore not emphasize the fit to this data set, but rather use it as an indicator of fit. The Ångerman river data is adjusted for eustatic sea level rise, using the curves by Fairbanks (1989) and Bard et al. (1990).

5 Comparison of GIA model predictions

In this section we analyze predictions from GIA models using the three ice-sheet reconstructions. We use two classes of earth models: one with uniform mantle viscosity and one with a 2-layered mantle viscosity structure, divided at 670 km depth into the upper and lower mantle. For the uniform viscosity models we explore the viscosity (η) vs. elastic thickness (T_{E}) parameter space, and for the 2-layer models we search the upper mantle viscosity (η_{um}) vs. lower mantle viscosity (η_{lm}) parameter space, assuming elastic thicknesses of 120, 140 and 160 km. In order to compare the GIA response from the three ice-sheet reconstructions we first study the fit of the predicted present day uplift rates to GPS observations, we then investigate the residual velocities, and finally we compare the predicted uplift curves to r.s.l. data for a few models.

5.1 GIA model fit to observed uplift rates

The χ_v^2 fit of the model predictions to the Lidberg et al. (2007) data is displayed in Fig. 6. Overall, we see that the misfit plots of the ANU models display a relatively simple topography of well fitting parameter values. For the UMISM and ICE-5G ice-sheets, the misfit of the 2-layer models are characterized by a doughnut shaped topography whereas the uniform viscosity models show curved contours of equal fit, with a well defined subregion of well fitting models. A similar feature can be seen in the misfit plots in Steffen et al. (2010) and Lidberg et al. (2010), as well as possibly hinted at in the misfit plots in Milne et al. (2004).

For the uniform viscosity models, ANU predicts the thinnest elastic thickness and the highest viscosity. The thickest elastic thickness is predicted by ICE-5G and the lowest viscosity by UMISM, and we note that the optimal subregions of UMISM and ICE-5G partly overlap. The elastic thickness predicted by ANU is in agreement with with the thickness range inferred from the construction of the ANU model (65–100 km, Lambeck et al., 2010). The greater thicknesses predicted by UMISM and ICE-5G are in agreement with the 160 km estimate by Steffen et al. (2010) although we note that this is significantly thicker than the 90 km assumed when constructing ICE-5G. Material parameters of the best fit uniform models are summarized in the uppermost block in Table 2 and the position of the best fit models are marked by yellow circles in Fig. 6.

For the 2-layer models only ANU predicts a reasonably well defined best fit model while the misfit plots of UMISM and ICE-5G suggest ranges of well fitting models. Even so, we present the model parameters that yields the lowest misfit in Table 2 and Fig. 6, knowing that these may be significantly influenced by our sampling of the parameter space. Although it appears from Table 2 that UMISM is the ice-sheet model that best fit the data, this could be due to under-sampling of the parameter space and such a conclusion cannot be drawn from these misfit plots. We note that the viscosity structure in the best fitting 2-layer ANU model agrees well with the optimal range resulting from the reconstruction of the ice-sheet (3–4 $\times 10^{20}$ and 5–20 $\times 10^{21}$ Pa s in the upper and lower mantle respectively, Lambeck et al., 2010). In the viscosity model VM2, used in the ICE-5G reconstruction, the mean viscosity in the upper and (uppermost) lower mantle are about 5×10^{20} and 1.6×10^{21} Pa s respectively. As indicated in Fig. 6 such an earth model will not be well fitted. However, if the VM2 mean viscosity in either the upper or the lower mantle is multiplied by a factor 2 the resulting earth model will be well fitted.

We have also analyzed the misfit to the 2010 BIFROST processing. In general we find the same features in the misfit plots based on this data set albeit slightly less pronounced. We further find that the viscosity of the best fit models change by less than a factor 2, generally towards greater viscosities in the uniform models and the upper mantle of the 2-layer models, while towards lower viscosities in the lower mantle.

Even though the misfit plots of the 2-layer models of UMISM and ICE-5G are similar in appearance, we note that the ICE-5G doughnut is slightly larger, with generally higher χ_v^2 values at the center, than the UMISM doughnut. We also find that the radius of the torus encompassing the well fitting region increases with decreasing elastic thickness. This can be observed in the misfit plot of ANU as well, which develops a doughnut feature when the elastic thickness decreases.

Analyzing the predicted velocities rather than the misfits we find that the greatest present day velocities are predicted by models at the center of the doughnut in parameter space. We further find that ICE-5G predicts the greatest uplift velocities followed by UMISM for identical earth models. This can be understood from the evolution of the ice-sheets seen in Fig. 2. ICE-5G displays a long history of a massive ice-sheet prior to LGM and is close to isostatic equilibrium when the deglaciation phase commences. UMISM has grown from almost ice-free conditions some 17 kyr before LGM and is far from isostatic equilibrium at LGM. Therefore less current uplift is predicted by UMISM. ICE-5G is further the most voluminous ice-sheet of the three reconstructions. The pre-LGM history of ANU is very similar to that of UMISM. However, the deglacia-

SED
5, 2345–2388, 2013

tion phase in ANU starts 2.8 kyr earlier in ANU than in UMISM therefore the rebound has proceeded furthest in ANU resulting in lower present day displacement rates.

5.1.1 Optimal viscosity bifurcation

The doughnut shaped region of well fitting models predicted by ICE-5G and UMISM can be readily understood from a simple model of postglacial uplift. During the rebound process, the vertical displacement, w, in a formerly glaciated region can be described by a function on the form (e.g Turcotte and Schubert, 2002)

$$w(\eta,t) = W \exp\left(-\frac{t}{A\eta}\right) \quad (2)$$

where W is a constant proportional to the maximum depression and A is a site specific constant. The vertical displacement rate is then given by a function on the form

$$v(\eta,t) = \frac{\mathrm{d}w}{\mathrm{d}t} = -\frac{W}{A\eta}\exp\left(-\frac{t}{A\eta}\right) \quad (3)$$

This function has a maximum velocity, $v^*(t)$ at a viscosity of

$$\eta^*(t) = \frac{t}{A} \quad (4)$$

The equations above show that at any given time t there exists a viscosity $\eta^*(t)$ that will give rise to the greatest uplift rate $v^*(t)$. If however the actual viscosity is either higher or lower than $\eta^*(t)$ the uplift rate will be smaller than $v^*(t)$. The time dependence of $\eta^*(t)$ is a reflection of the fact that a low viscosity earth will rebound fast, with the rebound velocity decaying fast with time. In a higher viscosity earth the initial rebound velocity is smaller but since the decay with time is slow, the rebound rate will eventually become faster than that in a low viscosity earth. In a multilayer model each viscous layer will have its own $v^*(t)$ and corresponding $\eta^*(t)$, potentially giving rise to a bifurcation in the optimal viscosity of each layer as seen in the ICE-5G and UMISM misfit plots. In the ANU case the predicted present day uplift rates are very close to v^*(now).

To investigate if the bifurcation arises from the use of the vertical displacement rates only, we have also generated similar plots based on the misfit of the full displacement vector. We find that the doughnut shaped region of well fitting ICE-5G and UMISM models is also present when the horizontal displacement rates are included, albeit a bit more diffuse, in agreement with the misfit plot presented in Lidberg et al. (2010).

5.2 Residual velocities

Figure 7 shows the residual velocities after subtraction of the predicted uplift rates from the BIFROST data. We see that the ANU model tends to under-predict velocities in Finland and northern Sweden and over-predict velocities in Denmark, and the southern halves of Norway and Sweden. ICE-5G on the contrary over-predicts velocities in eastern Finland, southern Norway and Denmark. The UMISM residuals show that the model over-predicts velocities in Denmark, southwestern Sweden and southern Norway and under-predicts velocities in central Sweden. These are general patterns that can be observed over a range of earth models for the respective ice-sheet reconstructions.

The high velocities over Finland in ICE-5G could be due to the late end of glaciation in this model, where the last remnants of the ice-sheet retracted to the northernmost part of the Gulf of Bothnia. In ANU and UMISM ice-free conditions are reached 1500–2000 yr earlier than in ICE-5G and the ice retreats to inland Sweden, and slightly further south in ANU. Likewise, the southwest-northeast trend of over- to under-prediction seen in ANU can be correlated to the more southwestern location of the ice centers in this reconstruction, causing higher uplift rates to the southwest and lower to the northeast.

Common to all three GIA models is an over-prediction at the stations in Denmark and at the station in Stavanger in southernmost Norway. This is most pronounced in the UMISM model, which has a relatively thick ice-bridge to the British isles. Such an ice-bridge is present around LGM in the ICE-5G model, although thinner and not as long lasting as in UMISM. We also note that in ANU, where no such ice-bridge exists around or after LGM, the Stavanger station is less over-predicted than the station at Trondheim, further north along the Norwegian coast. This is opposite to the predictions of UMISM and ICE-5G, where the over-prediction is greater at Stavanger than at Trondheim.

In most locations (about 85 %) for all three ice-sheets the residual velocities from the best fit models are below 1 mm yr^{-1}, and it is not possible to claim that one ice model is more successful than another from the fit to the GPS data alone.

Given the doughnut shaped subregion of reasonably well fitting models seen in the misfit plots of UMISM and ICE-5G, a comparison between the residuals of the best fit models alone might not be representative. We therefore also compare three well fitting UMISM and ICE-5G models with similar earth structure. We show the residual velocities for the chosen models in Fig. 8, as well as their location in parameter space as yellow triangles in Fig. 6.

In agreement with the best fit models above, the ICE-5G models consistently seem to over-predict the velocities over Finland, and all models over-predict velocities in Denmark and Stavanger, although this is more pronounced for the UMISM models. Further, the residuals in Denmark and Stavanger generally increase with increasing upper mantle viscosity. All models, except the ICE-5G model with stiffest lower mantle, over-predicts the velocities in southern Sweden with increasing residual velocities to the west. ICE-5G also tends to have slightly higher velocities at the two northernmost Norwegian stations than UMISM, possibly due to the more extensive ice-sheet over the Barents and Kara sea of ICE-5G.

5.3 Post glacial uplift history

Comparing the uplift histories predicted by the best fit uniform and 2-layer models (Table 2) at the Ångerman river, Sweden, (Fig. 9) we find significant differences. For the 2-layer models, UMISM predicts more than 163 m greater vertical displacement at 10 kyr BP than ICE-5G. The difference is less for the uniform viscosity models but still

SED
5, 2345–2388, 2013

amounts to about 75 m between ANU and UMISM. We note however that the uplift histories of the uniform UMISM and the 2-layer ANU are almost identical at this site. A further cross-examination of the uplift curves yields similar uplift curves for models of similar earth structure (Fig. 10). Figure 9 also displays the observed relative sea-level along the Ångerman river. We find that the uniform UMISM and the 2-layer ANU can fit this data within the given uncertainties while the 2-layer UMISM over-predicts the displacements and both the 2-layer and uniform ICE-5G as well as the uniform ANU under-predicts the displacements.

6 Summary and discussion

We have compared a thermo mechanical reconstruction of the Weichselian ice-sheet, UMISM, to two reconstructions based on the sea-level equation, ANU and ICE-5G, commonly used in GIA studies. Common to all three models are the use of dated ice-marginal positions in constraining the extent of the ice-sheet at different times although the data sets used varies between them. While UMISM is driven by palaeo-climatic data and focuses on physically viable ice-sheet dynamics, ANU and ICE-5G mainly focuses on matching observations of the post-glacial uplift by adjusting the thickness of the ice-sheet. The style of deglaciation in UMISM differs notably from ANU and ICE-5G both of which melt relatively uniformly over the entire ice-sheet while UMISM melts preferentially towards the edges. Whereas UMISM and ANU display a similar evolution in terms of integrated characteristics such as volume and areal extent, the fit of the displacements predicted by UMISM to observational data is more similar to that of ICE-5G. This is likely caused by the late timing of LGM in UMISM resulting in an about 2.8 kyr younger post-glacial phase than in ANU and therefore closer to the predictions of the more massive ICE-5G.

Despite a fundamentally different approach used in the reconstruction, UMISM can fit observational GIA data in Fennoscandia as well as both ANU and ICE-5G, both in terms of present day uplift rates and post glacial uplift history. It is therefore not feasible

SED
5, 2345–2388, 2013

to claim one reconstruction to be more successful than the others in reproducing the GIA observations we have used herein. Although, based primarily on physical principles rather than inversion of GIA data, the UMISM reconstruction is bound to evolve as a real ice-sheet, which is not the case for neither the ICE-5G nor the ANU reconstructions. In addition, the modeling of the earth response is handled in a simplified way in UMISM. This indicates a slightly lower degree of coupling between the earth and the ice model than offered by ICE-5G and ANU, as the reconstruction in these latter two models largely rests on a proper modelling of the earth response. We note that the ANU reconstruction includes an inversion for the optimal earth model parameter ranges while ICE-5G assumes these to be a priori known.

Implemented in a GIA model, ICE-5G is close to isostatic equilibrium at LGM while both ANU and UMISM, having grown from small ice-sheets prior to LGM, are far from isostatic equilibrium. Therefore the pre-LGM development of the Weichselian ice-sheet needs to be considered when using ANU or UMISM in GIA modelling. We find that changes in the reconstructions prior to 36 kyr BP affects the predicted present day uplift rates by less than 0.1 $\mathrm{mm\,yr^{-1}}$. The predicted postglacial displacement curve is however more affected. At the Ångerman river, close to the center about 30 m due to changes in of the ice-sheet, the vertical displacement 10 kyr BP may differ by up to the ice-sheet prior to 36 kyr BP, while changes prior to 55 kyr BP affects the displacement by less than 5 m. Hence if comparing the model predictions to rsl data a longer history of the ANU and UMISM ice-sheets needs to be taken into consideration.

Given identical earth models we find that ICE-5G in general predicts the fastest present day uplift rates and ANU the slowest. Analyzing the residual velocities for well fitted earth models, with emphasis on trends independent of the earth model, we find that improvements can be made in all three reconstructions. In particular, we find that ICE-5G tends to over-predict the velocities over Finland while ANU tend to under-predict them. Although inspection of the respective ice-sheets shows that the post-LGM ice-sheet in ANU is relatively thin over Finland while ICE-5G displays a thick ice coverage over Finland, stretching well into western most Russia, this may not be the sole explanation. Also the post-LGM ice-sheet in UMISM is relatively thick over Finland and western most Russia, yet the predicted uplift velocities in Finland lies in between those predicted by ANU and ICE-5G. Common to UMISM and ANU is instead a continuation of the ice-thickness south of Finland whereas in ICE-5G a clear divide is seen along the southern border of Finland with great ice-thicknesses to the north and thin ice to the south. Further, the center of the ice-sheet in both UMISM and ANU migrates westward in the last stages of the deglaciation phase whilst in ICE-5G the center stays more or less fixed over the Gulf of Bothnia. It is therefore likely that while ANU would benefit from greater post-LGM thickness to the east, ICE-5G would benefit slightly reduced thickness over inland Finland and greater post-LGM thickness over the southern half of the Baltic sea and the western shores of the Baltic states, as well as a west-ward migration of the ice-center in the final stages of deglaciation.

UMISM generally under-predicts the velocities over central to northern Sweden and similar trends can also be seen in ANU and ICE-5G. We further find that for most of the well fitting earth models, all ice models tend to predict slightly too high velocities in southwestern Fennoscandia, in particular in Denmark and southernmost Norway. This may indicate that the center of mass in all three reconstructions at LGM and onwards is placed slightly to far south.

A clear difference in the trend of the residual velocities along the southern Norwegian coast can be seen between the predictions of ANU and the predictions of UMISM and ICE-5G. This is interpreted as due to the extensive ice-bridge to the British isles in both ICE-5G and UMISM during LGM and the early deglaciation phase. As an ice-bridge is absent in ANU during this time period, more GPS stations along the southern coast of Norway may help in constraining the past existence of such a feature.

The range of preferred elastic thicknesses differs significantly between the ice models, with ANU at the thinner end (< 100 km) and ICE-5G at the ticker end (140–250 km). We generally find slightly lower misfits for models with a viscosity contrast over the boundary between the upper and lower mantle than for models with a uniform mantle viscosity. However, only for ANU can a single best fitting earth model be reasonably

SED
5, 2345–2388, 2013

well constrained in the 2 layer models. For the faster present day uplift rates in UMISM and ICE-5G, a bifurcation in the optimal viscosity in both the upper and lower mantle results in a doughnut shaped region in parameter space of well fitting earth models. As the objective of this study is not to find the optimal ice or earth model but instead a comparison of three rather different ice-sheet reconstructions we have not included the horizontal component of the surface displacements in our analysis above. Investigating the effect of also including the horizontals we find that this would help constraining the preferred elastic thickness for all three ice-sheet but not single out an optimal reconstruction. Moreover, this would this would not remove the ambiguity seen in the doughnut shaped region of well fitted models for UMISM or ICE-5G (see e.g. Fig. 6 in Lidberg et al., 2010). It is therefore desirable to include other observations of the postglacial uplift such as relative sea level curves in the analysis to better constrain the earth parameters. Our comparison of the uplift history for well fitting models indicate that this could resolve the observed ambiguity.

7 Conclusions

We find that while the characteristics of the UMISM reconstruction is more similar to ANU, the predicted post-glacial uplift and fit to present day uplift rates is more similar to those predicted by ICE-5G. The present day uplift velocities predicted by UMISM are intermediate between those predicted by ICE-5G (fastest) and ANU (slowest) given identical earth models. But more importantly, given appropriate earth models the predictions by UMISM fit observational data equally well as the predictions by ANU and ICE-5G. We note that only ANU yield a relatively well constrained best fit model when compared to observed present day uplift rates. Whereas for both ICE-5G and ANU bifurcations in the optimal upper and lower mantle viscosity gives rise to a range of well fitting models. However, it is not possible to claim one model better than the others in reproducing the post-glacial uplift process, based on the observational data used herein, UMISM has the benefit of being based on thermo-mechanical modelling and therefore a physically viable reconstruction, this is not necessarily the case in neither ANU nor ICE-5G where the ice-sheet has been optimized to yield post-glacial uplift curves in accordance with observations. Moreover, given the large difference between ICE-5G and ANU ice-sheets it is clear that there exists a large freedom in reconstructing the Weichselian ice-sheet based on an optimization to observational r.s.l. data. We find that improvements can be made to all three reconstructions to better fit the observed present day uplift rates. More specifically, the post-LGM ice-sheet in ANU would benefit from greater thickness to the east while the post-LGM ice-sheet in ICE-5G would benefit from reduced thickness over Finland, increased thickness over the southern half of the Baltic sea and the western shores of the Baltic states and a west-ward migration of the ice-center in the final stages of deglaciation. In addition, in all three reconstructions, the mass center of the ice-sheet appears to be located slightly to far south from LGM and onwards.

Acknowledgements. The authors thank Kurt Lambeck for giving us access to the latest ANU reconstruction of the Weichselian ice-sheet. We further thank Hans-Georg Scherneck for help on rotating the horizontal component of the predicted displacements as displayed in Figs. 7 and 8. PS and BL thanks the Swedish Nuclear Fuel and Waste Management Co (SKB) for financial support in early parts of this work. All figures were produced using the freely available, open source software GMT (Wessel and Smith, 1991).

References

Bard, E., Hamelin, B., Fairbanks, R. G., and Zindler, A.: Calibration of ^{14}C over the last 30 000 years using U/Th ages obtained by mass spectrometry on Barbados coral, Nature, 345, 405–410, doi:10.1038/345405a0, 1990. 2349, 2359

Boulton, G., Dongelmans, P., Punkari, M., and Broadgate, M.: Palaeoglaciology of an ice sheet through a glacial cycle: the European ice sheet through the Weichselian, Quarternary Sci. Rev., 20, 591–625, doi:10.1016/S0277-3791(00)00160-8, 2001. 2349

Cato, I.: Shore displacement data based on lake isolations confirm the postglacial parts of the Swedish Geochronological Time Scale, Sveriges Geologiska Undersökning, 75–80, 1992. 2348, 2359

Dansgaard, W., Johnsen, S. J., Clausen, H. B., Dahl-Jensen, D., Gundestrup, N. S., Hammer, C. U., Hvidberg, C. S., Steffensen, J. P., Sveinbjörnsdottir, A. E., Jouzel, J., and Bond, G.: Evidence for general instability of past climate from a 250-kyr ice-core record, Nature, 364, 218–220, doi:10.1038/364218a0, 1993. 2350

Drewry, D. J. (Ed.): Antarctica: Glaciological and Geophysical Folio, Scott Polar Res. Inst., Cambridge, 1982. 2352

Dziewonski, A. M. and Anderson, D. L.: Preliminary reference Earth model, Phys. Earth Planet. In., 25, 297–356, doi:10.1016/0031-9201(81)90046-7, 1981. 2353, 2357, 2375

Ekman, M.: A concise history of postglacial land uplift research (from its begining to 1950), Terra Nova, 3, 358–365, doi:10.1111/j.1365-3121.1991.tb00163.x, 1991. 2347

Fairbanks, R. G.: A 17 000-year glacio-eustatic sea level record: influence of glacial melting rates on the younger Dryas event and deep-ocean circulation, Nature, 342, 637–642, doi:10.1038/342637a0, 1989. 2359

Fastook, J. L.: Modelling the ice age: the finite-element method in glaciology, IEEE Comp. Sci. Eng., 1, 55–67, doi:10.1109/99.295374, 1994. 2349

Fastook, J. L. and Chapman, J. E.: A map-plane finite-element model – 3 modeling experiments, J. Glaciol., 35, 48–52, doi:10.3189/002214389793701464, 1989. 2349

Fastook, J. L. and Prentice, M.: A finite-element model of Antarctica – sensitivity test for meteorological mass-balance relationships, J. Glaciol., 40, 167–175, 1994. 2349, 2350

Hughes, T. J., Denton, G. H., Anderson, B. G., Schilling, D. H., Fastook, J. L., and Lingle, C. S.: The last great ice sheets: a global view, in: The Last Great Ice Sheets, edited by: Denton, G. H. and Hughes, T. J., John Wiley and Sons, New York, 263–317, 1981. 2352

Huybrechts, P., Payne, T., and The EISMINT Intercomparison Group: The EISMINT benchmarks for testing ice-sheet models, Ann. Glaciol., 23, 1–12, 1996. 2349

Johnson, J. V.: A basal water model for ice sheets, Ph. D. thesis, The University of Maine, publication Number: AAI3057580; ISBN: 9780493729091, 1994. 2350

Lambeck, K.: Glacial rebound of the British Isles – II. A high-resolution, high precision model, Geophys. J. Int., 115, 960–990, doi:10.1111/j.1365-246X.1993.tb01504.x, 1993. 2352

Lambeck, K.: Late devensian and holocene shorelines of the British Isles and North Sea from models of glacio-hydro-isostatic rebound, J. Geol. Soc., 152, 437–448, doi:10.1144/gsjgs.152.3.0437, 1995. 2352

Lambeck, K.: Limits on the areal extent of the Barents Sea ice sheet in Late Weichselian time, Global Planet. Change, 12, 41–51, doi:10.1016/0921-8181(95)00011-9, 1996. 2353

Lambeck, K., Smither, C., and Johnston, P.: Sea-level change, glacial rebound and mantle viscosity for northern Europe, Geophys. J. Int., 134, 102–144, doi:10.1046/j.1365-246x.1998.00541.x, 1998. 2348, 2352

Lambeck, K., Purcell, A., Funder, S., Kjær, K. H., Larsen, E., and Möller, P.: Constraints on the Late Saalian to early Middle Weischelian ice sheet of Eurasia from field data and rebound modelling, BOREAS, 35, 539–575, doi:10.1080/03009480600781875, 2006. 2353

Lambeck, K., Purcell, A., Zhao, J., and Svensson, N.-O.: The Scandinavian ice sheet: from MIS 4 to the end of the last glacial maximum, BOREAS, 39, 410–435, doi:10.1111/j.1502-3885.2010.00140.x, 2010. 2348, 2353, 2360, 2361

Lidberg, M., Johansson, J. M., Scherneck, H.-G., and Davis, J. L.: An improved and extended GPS-derived 3D velocity field of the glacial isostatic adjustment (GIA) in Fennoscandia, J. Geodesy, 81, 213–230, doi:10.1007/s00190-006-0102-4, 2007. 2348, 2358, 2360, 2383, 2385, 2386

Lidberg, M., Johansson, J. M., Scherneck, H.-G., and Milne, G. A.: Recent results based on continous GPS observations of the GIA process in Fennoscandia from BIFROST, J. Geodyn., 50, 8–18, doi:10.1016/j.jog.2009.11.010, 2010. 2358, 2360, 2363, 2368

Lidén, R.: Den senkvartära strandförskjutningens förlopp och kronologi i Ångermanland., Geol. Foren. Stock. For., 60, 397–404, 1938. 2348, 2359

Lokrantz, H. and Sohlenius, G.: Ice marginal fluctuations during the Weichselian glaciation in Fennoscandia, a literature review, Tech. Rep. TR-06-36, Swedish Nuclear Fuel and Waste Management Co. (SKB), Stockholm, Sweden, 2006. 2350

Lund, B., Schmidt, P., and Hieronymus, C.: Stress evolution and fault stability during the Weichselian glacial cycle, Tech. Rep. TR-09-15, Swedish Nuclear Fuel and Waste Management Co. (SKB), Stockholm, Sweden, 2009. 2350

Martinson, D. G., Pisias, N. G., Hays, J. D. Imbrie, J., Moore Jr, T. C., and Shackleton, N. J.: Age dating and orbital theory of the ice ages: development of a high resolution 0–300 000-year chronostratigraphy, Quarternary Sci. Rev., 27, 1–30, doi:10.1016/0033-5894(87)90046-9, 1987. 2352

Milne, G. A., Mitrovica, J. X., Scherneck, H.-G., Davis, J. L., Johansson, J. M., Koivula, H., and Vermeer, M.: Continuous GPS measurements of postglacial adjustment in Fennoscandia: 2. Modeling results, J. Geophys. Res., 109, B02412, doi:10.1029/2003JB002619, 2004. 2360

Nakada, M. and Lambeck, K.: Glacial rebound and relative sea-level variations: a new appraisal, Geophys. J. Roy. Astr. S., 90, 171–224, doi:10.1111/j.1365-246X.1987.tb00680.x, 1987. 2352

Nakada, M. and Lambeck, K.: The melting history of the late Pleistocene Antarctic ice sheet, Nature, 333, 36–40, doi:10.1038/333036a0, 1988. 2352

Nakada, M. and Lambeck, K.: Late Pleistocene and Holocene sea-level change in the Australian region and mantle rheology, Geophys. J., 96, 497–517, doi:10.1111/j.1365-246X.1989.tb06010.x, 1989. 2352

Näslund, J.-O.: Ice sheet dynamics, in Climate and climate-related issues for the safety assesment SR-Site., Tech. Rep. TR-10-49, Swedish Nuclear Fuel and Waste Management Co. (SKB), Stockholm, Sweden, 2010. 2348, 2349, 2350

Näslund, J.-O., Jansson, P., Fastook, J. L., Johnson, J., and Andersson, L.: Detailed spatially distributed geothermal heat-flow data for modeling of basal temperatures and meltwater production beneath the Fennoscandian ice sheet, Ann. Glaciol., 40, 95–101, doi:10.3189/172756405781813582, 2005. 2350

Paterson, W. S. B.: The Physics of Glaciers, Pergamon, New York, 480 pp., 1994. 2353

Payne, A. J., Huybrechts, P., Abe-Ouchi, A., Calov, R., Fastook, J. L., Greve, R., Marshall, S. J., Marsiat, I., Ritz, C., Tarasov, L., and Thomassen, M. P. A.: Results from the EISMINT model intercomparison: the effects of thermomechanical coupling, J. Glaciol., 46, 227–238, doi:10.3189/172756500781832891, 2000. 2349

Peltier, W. R.: Ice age paleotopography, Science, 265, 195–201, doi:10.1126/science.265.5169.195, 1994. 2351

Peltier, W. R.: Mantle viscosity from the simultaneous inversion of multiple data sets pertaining to postglacial rebound, Geophys. Res. Lett., 23, 503–506, doi:10.1029/96GL00512, 1996. 2351, 2352

Peltier, W. R.: Postglacial variations in the level of the sea: implications for climate Dynamics and solid-earth geophysics, Rev. Geophys., 36, 603–689, doi:10.1029/98RG02638, 1998. 2351

SED
5, 2345–2388, 2013

Peltier, W. R.: Global glacial isostacy and the surface of the ice-age earth: the ICE-5G (VM2) model and GRACE, Annu. Rev. Earth Pl. Sc., 32, 111–149, doi:10.1146/annurev.earth.32.082503.144359, 2004. 2348, 2351, 2352

Peltier, W. R. and Andrews, J. T.: Glacial-isostatic adjustment – I. The forward problem, Geophys. J. Roy. Astr. S., 46, 605–646, 1976. 2351

Peltier, W. R. and Fairbanks, R. G.: Global glacial ice volume and last glacial maximum duration from an extended Barbados sea level record, Quarternary Sci. Rev., 25, 3322–3337, doi:10.1016/j.quascirev.2006.04.010, 2006. 2352

Plag, H. P., Engen, B., Clark, T. A., Degnan, J. J., and Richter, B.: Post-glacial rebound and present-day three-dimensional deformations, J. Geodyn., 25, 263–301, doi:10.1016/S0264-3707(97)00032-X, 1998. 2347

Schmidt, P., Lund, B., and Hieronymus, C.: Implementation of the glacial rebound pre-stress advection correction in general-purpose finite element analysis software: springs versus foundations, Computat. Geosci., 40, 97–106, doi:10.1016/j.cageo.2011.07.017, 2012. 2357

Schotman, H. H. A., Wu, P., and Vermeersen, L. L. A.: Regional perturbations in a global background model of glacial isostacy, Phys. Earth Planet. In., 171, 323–335, doi:10.1016/j.pepi.2008.02.010, 2008. 2356, 2357

Spada, G., Barletta, V. R., Klemann, V., Riva, R. E. M., Martinec, Z., Gasperini, P., Lund, B., Wolf, D., Vermeersen, L. L. A., and King, M. A.: A benchmark study for glacial isostatic adjustment codes, Geophys. J. Int., 185, 106–132, doi:10.1111/j.1365-246X.2011.04952.x, 2011. 2357

Steffen, H. and Wu, P.: Glacial isostatic adjustment in Fennoscandia – a review of data and modeling, J. Geodyn., 52, 169–204, doi:10.1016/j.jog.2011.03.002, 2011. 2347

Steffen, H., Wu, P., and Wang, H.: Determination of the Earth's structure in Fennoscandia from GRACE and implications for the optimal post-processing of GRACE data, Geophys. J. Int., 182, 1295–1310, doi:10.1111/j.1365-246X.2010.04718.x, 2010. 2348, 2360

Toscano, M. A., Peltier, W. R., and Drummond, R.: ICE-5G and ICE-6G models of postglacial relative sea-level history applied to the Holocene coral reef of northeastern St Croix, U.S.V.I.: investigating the influence of rotational feedback on GIA processes at tropical latitudes, Quarternary Sci. Rev., 30, 3032–3042, doi:10.1016/j.quascirev.2006.04.010, 2011. 2351

Turcotte, D. L. and Schubert, G.: Geodynamics, 2nd edn., Cambridge University Press, Cambridge, 2002. 2362

Tushingham, A. M. and Peltier, W. R.: Ice-3G: a new global model of late Pleistocene deglaciation based upon geophysical predictions of post-glacial relative sea level change, J. Geophys. Res., 96, 4497–4523, doi:10.1029/90JB01583, 1991. 2351

Wessel, P. and Smith, W. H. F.: Free software helps map and display data, EOS T. Am. Geophys. Un., 72, 441, doi:10.1029/90EO00319, 1991. 2369

Whitehouse, P.: Isostatic adjustment and shoreline migration, in climate and climate-related issues for the safety assesment SR-Can., Tech. Rep. TR-06-23, Swedish Nuclear Fuel and Waste Management Co. (SKB), Stockholm, Sweden, 2006. 2350

Whitehouse, P.: Glacial isostatic adjustment and sea-level change, State of the art report, Tech. Rep. TR-09-11, Swedish Nuclear Fuel and Waste Management Co. (SKB), Stockholm, Sweden, 2009. 2347

Wu, P.: Using commercial finite element packages for the study of earth deformations, sea levels and the state of stress, Geophys. J. Int., 158, 401–408, doi:10.1111/j.1365-246X.2004.02338.x, 2004. 2356

Wu, P. and Peltier, W. R.: Glacial isostatic adjustment and the free air gravity anomaly as a constraint on deep mantle viscosity, Geophys. J. Roy. Astr. S., 74, 377–449, 1983. 2352

Table 1. Elastic material parameters and densities used in the earth models as derived from volume averages of PREM (Dziewonski and Anderson, 1981).

Layer	Depth [km]	Density [$kg\,m^{-3}$]	Young's [GPa]	Poisson's ratio	Rheology
1	15	2750	64	0.28	Elastic
2	50	3251	156	0.28	Elastic
3	80–280	3378	170	0.28	Elastic
4	410	3433	182	0.28	Viscoelastic
5	670	3837	263	0.28	Viscoelastic
6	∞	4853	552	0.28	Viscoelastic

SED
5, 2345–2388, 2013

SED

5, 2345–2388, 2013

Weichselian ice sheet reconstructions

P. Schmidt et al.

Table 2. Parameters for the earth models that best fit the BIFROST vertical velocities, from Fig. 6, for all three ice-sheet reconstructions. Upper block shows results from uniform mantle viscosity models and the lower three blocks shows results from 2-layer mantle viscosity models, for elastic thicknesses of 120, 140, and 160 km. The overall best fit model of each ice-sheet reconstruction is highlighted in bold.

Ice	T_e [km]	η_{um} [10^{20} Pa s]	η_{lm} [10^{20} Pa s]	χ_v^2
ANU	80	35		23.73
UMISM	140	15		17.50
ICE-5G	200	25		16.40
ANU		**5**	**100**	**14.93**
UMISM	120	**5**	**30**	**11.51**
ICE-5G		30	200	17.21
ANU		10	50	18.94
UMISM	140	20	150	13.97
ICE-5G		**20**	**300**	**14.48**
ANU		10	50	17.52
UMISM	160	10	300	13.64
ICE-5G		10	500	15.68

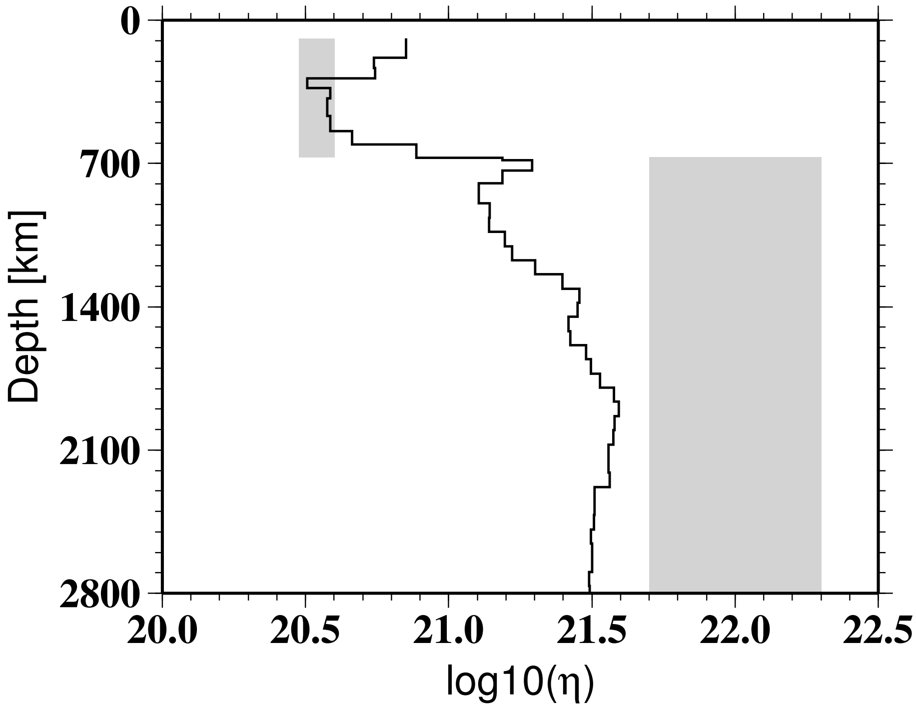

Fig. 1. Viscosity profile VM2 (black line) used in the ICE-5G reconstruction and optimal 2-layer viscosity range (gray regions) found in the ANU reconstruction.

SED
5, 2345–2388, 2013

Weichselian ice sheet reconstructions

P. Schmidt et al.

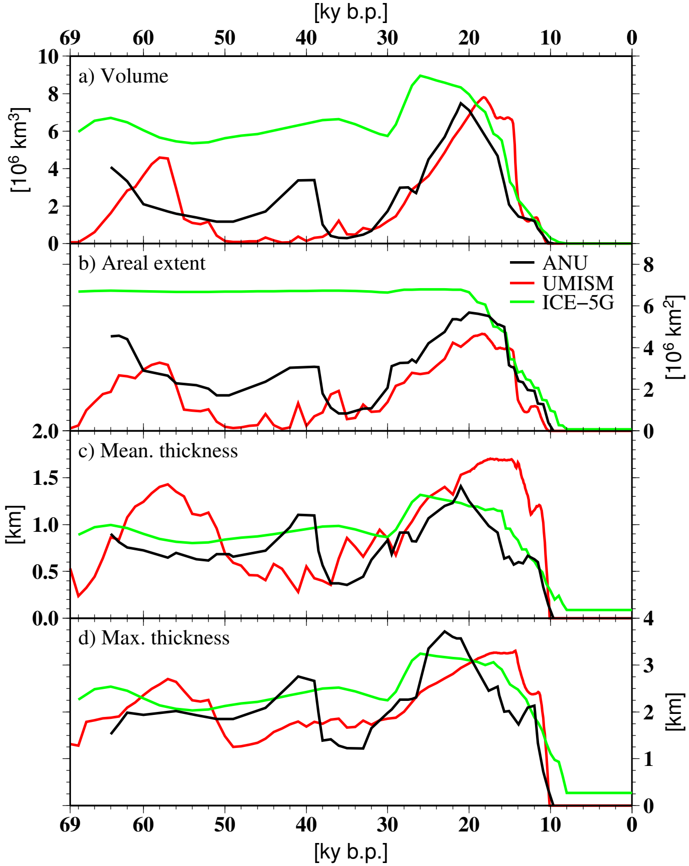

Fig. 2. (a) Ice volume, **(b)** areal extent, **(c)** mean thickness and **(d)** maximum thickness of the UMISM (red), ICE-5G (green) and ANU (black) ice-sheet reconstructions. The termination of the curves at early times represents the snapshots closest in time to 69 kyr BP simulation start. The non-zero thickness in ICE-5G from about 8 kyr BP until today is associated with a non-vanishing small ice cover in the northernmost part of Nova Zemlya, Russia.

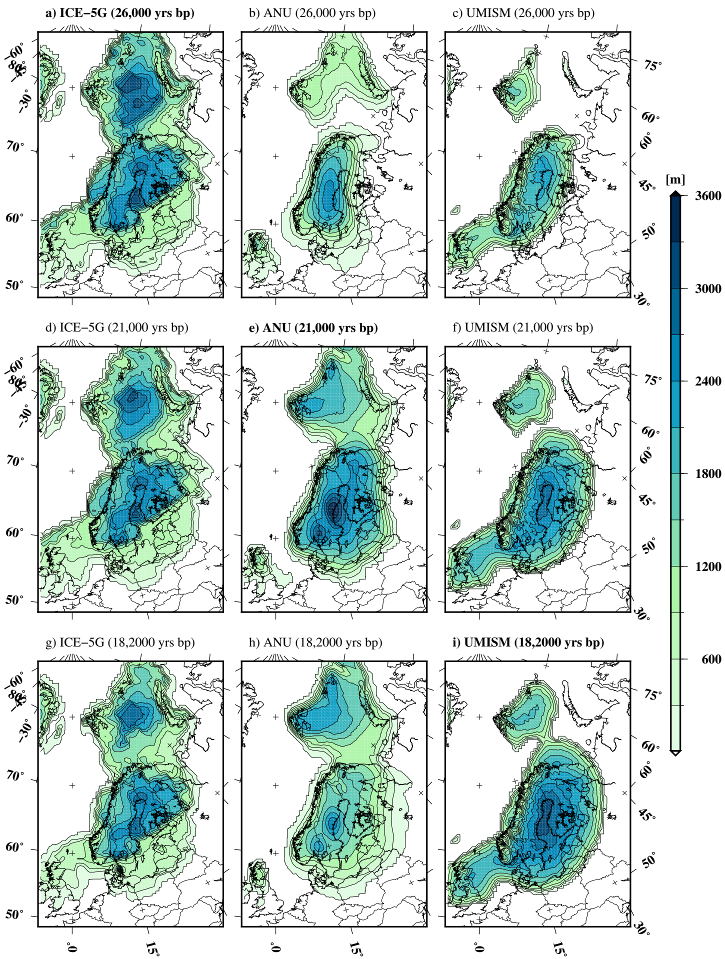

Fig. 3. Caption on next page.

Fig. 3. Ice sheet extent and thickness at 26 kyr BP (**a–c**, LGM of ICE-5G), 21 kyr BP (**d–f**, LGM of ANU), and 18 200 BP (**g–i**, LGM of UMISM) for ICE-5G (**a**, **d** and **g**), ANU (**b**, **e** and **h**) and the UMISM model (**c**, **f** and **i**). Bold font header indicates LGM of respective ice-sheet reconstruction (**a**, **e** and **i**). ICE-5G and ANU ice thicknesses at 18.2 kyr BP have been linearly interpolated from adjacent time frames (16.5 and 20 kyr BP for ANU, 18 and 19 kyr BP for ICE-5G), while the extents have been inherited from the closest preceding snapshot.

SED
5, 2345–2388, 2013

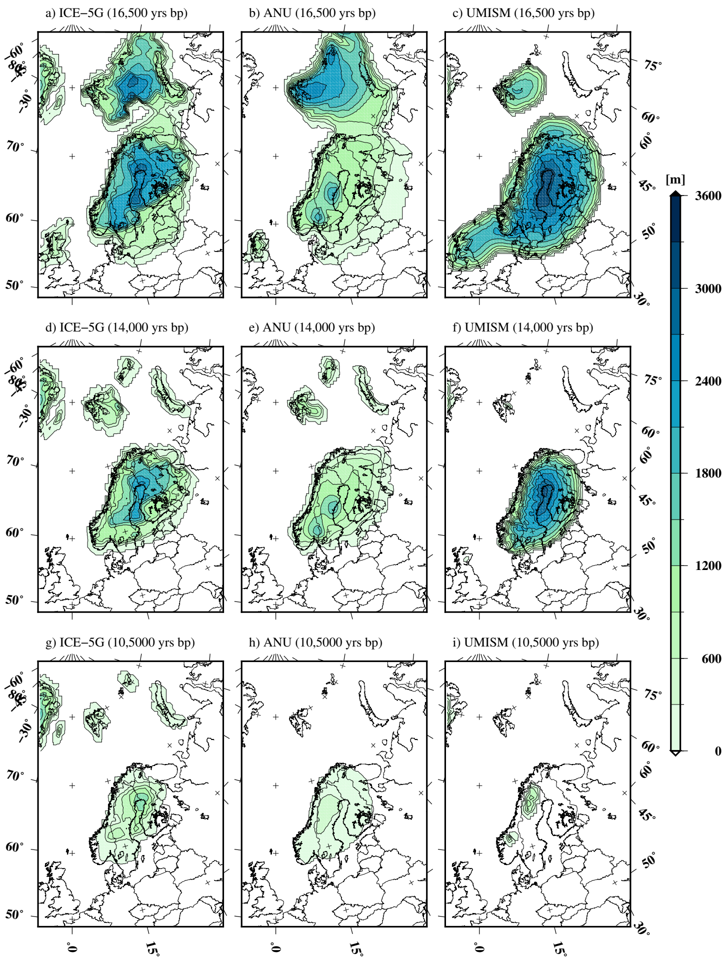

Fig. 4. Caption on next page.

Fig. 4. Ice sheet extent and thickness at 16.5 kyr BP **(a–c)**, 14 kyr BP **(d–f)**, and 10.5 kyr BP **(g–i)** for ICE-5G (**a**, **d** and **g**), ANU (**b**, **e** and **h**) and the UMISM model (**c**, **f** and **i**). Note that the ANU model at 10.5 kyr BP has been generated by linear interpolation in thickness between the solution at 10 910 and 10 274 yr BP, the extent of the ice-sheet is inherited from 10 910 yr BP, while the ice-sheet displayed at 14 kyr BP is the snapshot at 13 940 yr BP.

SED

5, 2345–2388, 2013

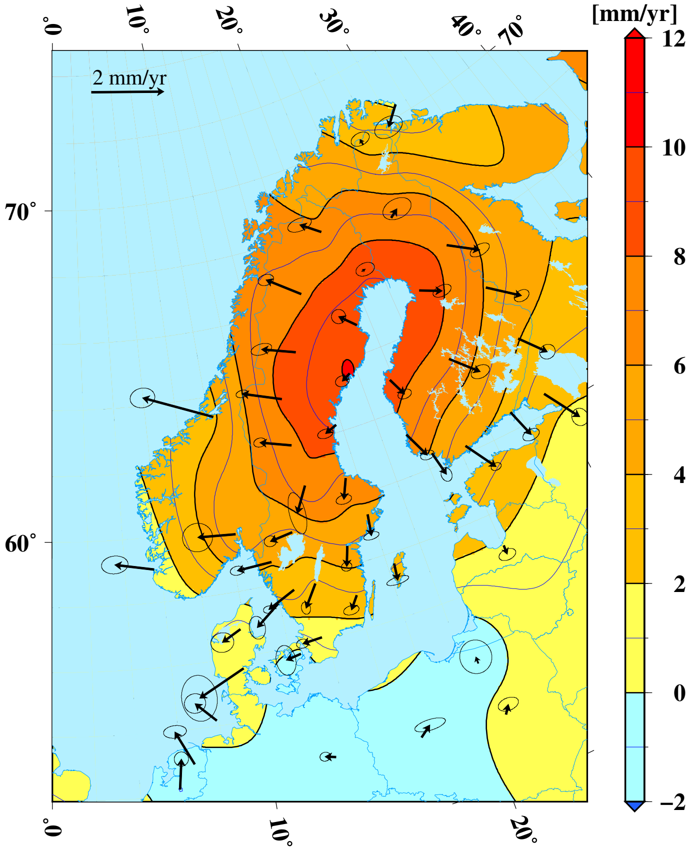

Fig. 5. Present vertical (color contours) and horizontal (vectors with uncertainty ellipses) surface velocities in Fennoscandia, as measured by GPS in the BIFROST project (Lidberg et al., 2007).

SED
5, 2345–2388, 2013

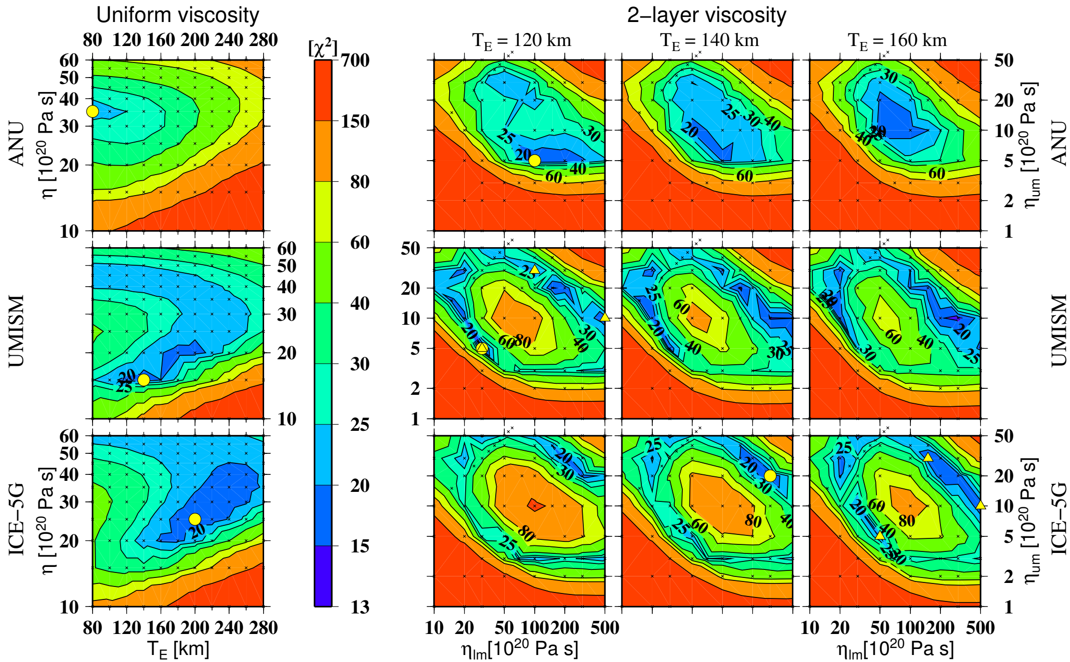

Fig. 6. χ^2_ν fit to the vertical displacement rates of the BIFROST data for GIA models using the ANU (upper row), ICE-5G (middle row) or UMISM (lower row) ice-sheet reconstructions. Left column displays the fit of the uniform viscosity models as a function of mantle viscosity (η) and the elastic thickness of the lithosphere (T_E). The right 3 × 3 block shows the fit of the 2-layer models as a function of upper mantle and lower mantle viscosities (η_{um} and η_{lm}) and elastic thickness of the lithosphere of 120 km (left column of block), 140 km (middle) and 160 km (right). Tiny "x" mark the locations of tested parameter combinations, yellow circles mark the locations of best fit models and yellow triangles mark the location of the UMISM and ICE-5G models compared in Fig. 8.

SED
5, 2345–2388, 2013

Weichselian ice sheet reconstructions

P. Schmidt et al.

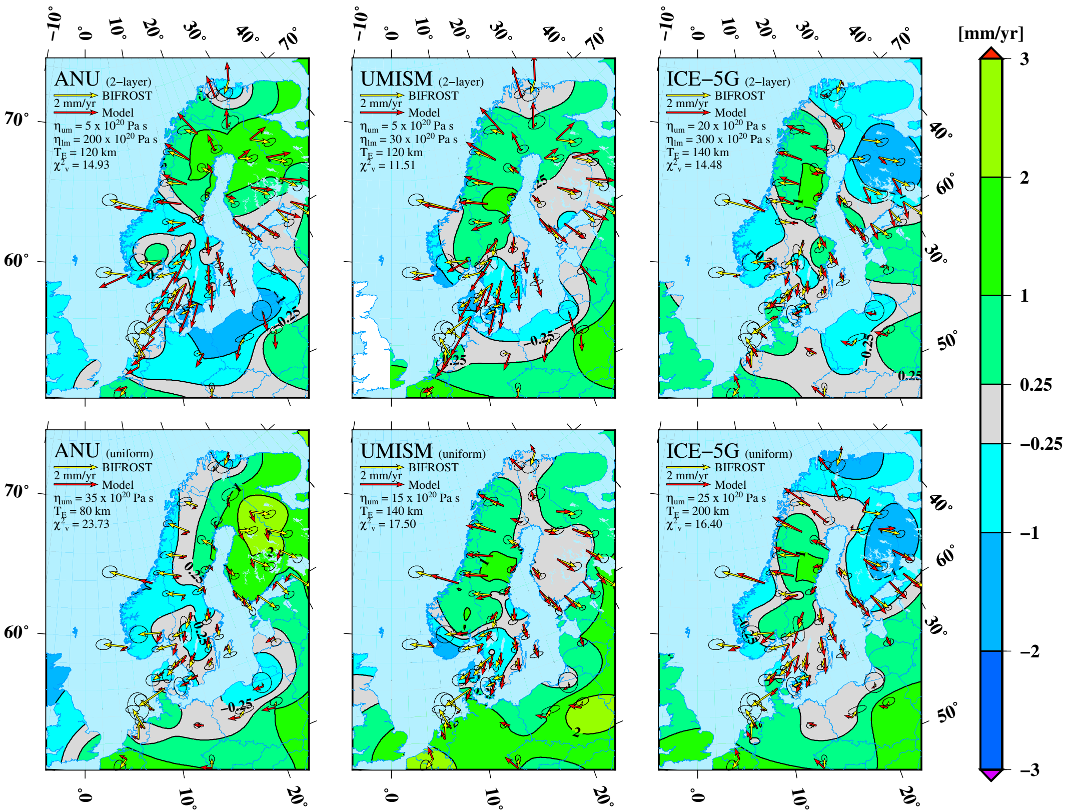

Fig. 7. Residual vertical velocities after subtraction from the BIFROST observations of the best fit 2-layer models (upper row) and uniform viscosity models (lower row) of ANU (left), UMISM (middle), and ICE-5G (right). Negative residual (blue colors) indicate too fast model predictions. Also shown are observed (yellow vectors) and predicted (red vectors) horizontal velocities, the latter adjusted by a rigid rotation as explained in Lidberg et al. (2007).

SED
5, 2345–2388, 2013

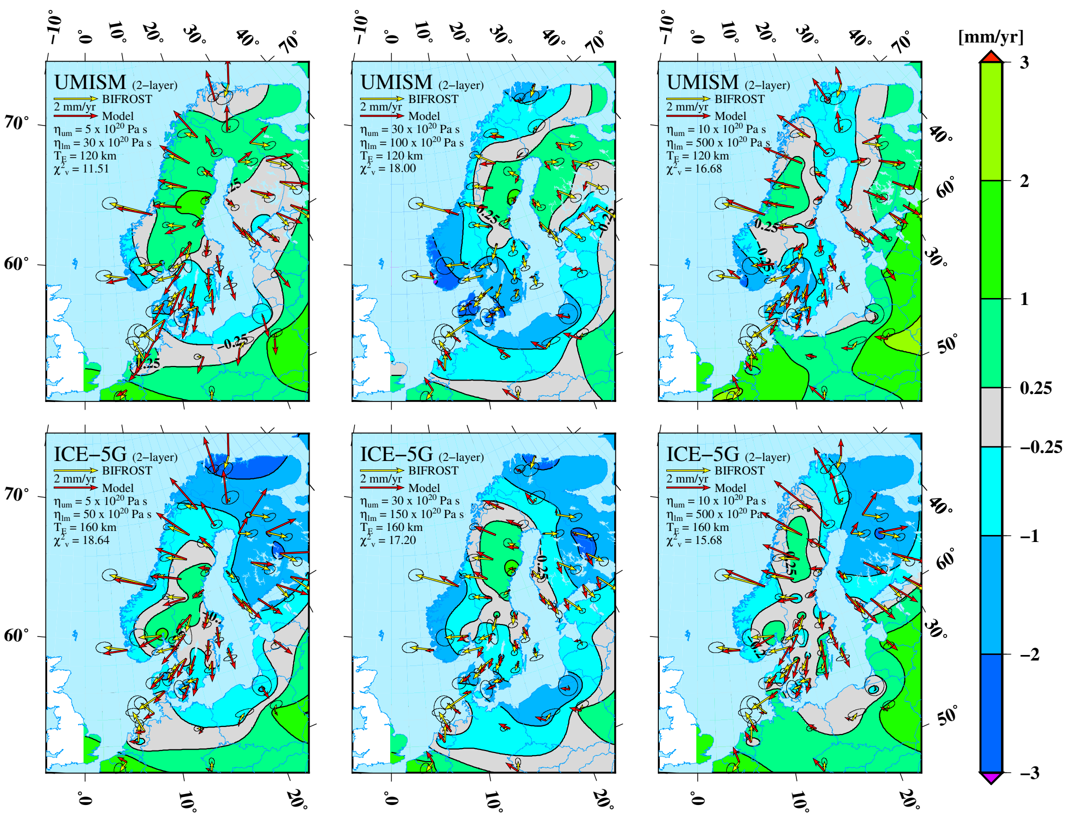

Fig. 8. Residual vertical velocities after subtraction from the BIFROST observations of selected well fitting uniform viscosity models of UMISM (upper row), and ICE-5G (lower row). Negative residuals (blue colors) indicate too fast predictions. Earth model parameters are shown in the legends. Also shown are observed (yellow vectors) and predicted (red vectors) horizontal velocities, the latter adjusted by a rigid rotation as explained in Lidberg et al. (2007).

SED
5, 2345–2388, 2013

Weichselian ice sheet reconstructions

P. Schmidt et al.

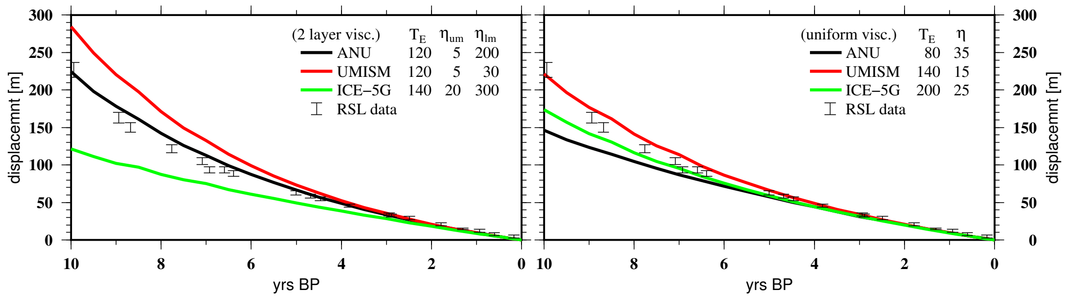

Fig. 9. Relative displacements at the Ångerman river, Sweden, predicted by the best fit 2-layer models (left panel) and uniform viscosity models (right panel). For comparison the r.s.l. data collected along the Ångerman river are shown with error bars in the graph. The legends show elastic thickness, T_E, in km and viscosities, η,in units of 10^{20} Pa s.

SED
5, 2345–2388, 2013

Weichselian ice sheet reconstructions

P. Schmidt et al.

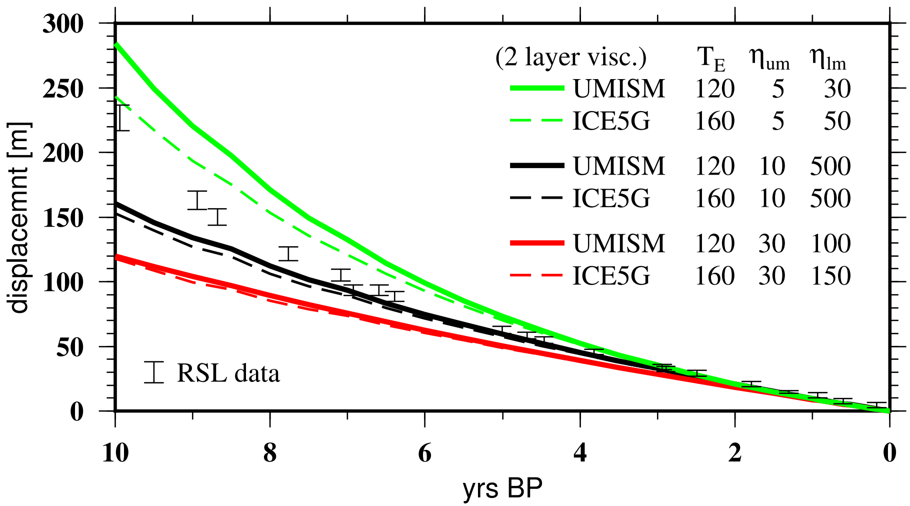

Fig. 10. Predicted relative displacement curves along the Ångerman river from selected uniform viscosity models of UMISM and ICE-5G. For comparison the Ångerman river r.s.l. data are shown with error bars in the graph. The legends show elastic thickness, T_E, in km and viscosities, η,in units of 10^{20} Pa s.

SED
5, 2345–2388, 2013